ORIGINAL CONTRIBUTION

Contact angle hysteresis at the nanoscale: a molecular dynamics simulation study

Feng-Chao Wang · Ya-Pu Zhao

Abstract In this paper, the contact angle hysteresis (CAH) of nanodroplets on both rigid and flexible substrates with different wettabilities was studied using molecular dynamics (MD) simulations. The critical shear stress (CSS) that determines the motion of the contact line (CL) was investigated. A theoretical correlation between CAH and CSS was proposed. Both CAH and CSS reflect the energy dissipation at the CL of the droplet in response to the exerted force. MD results of CAH are qualitatively consistent with the theoretical model. Simulation results also show that, for the same liquid–solid interactions, CAH on the flexible substrate is larger than that on the rigid substrate. These findings aim to enhance our understanding of the mechanism of the CAH at the nanoscale.

Notations
θ Contact angle
γ Surface tension
ε Depth of the potential well
σ Effective molecular diameter
τ_c Critical shear stress
h^* Height of the ridge

G Shear modulus of the substrate
E_0 Height of the energy barrier
k_B The Boltzmann constant
T The absolute temperature
R Droplet base radius

Subscripts
l   Liquid
s   Solid
v   Vapor
r   Receding angle
a   Advancing angle

Abbreviations
CA   Contact angle
CAH   Contact angle hysteresis
CSS   Critical shear stress
CL   Contact line
MD   Molecular dynamics
LJ   Lennard–Jones

F.-C. Wang · Y.-P. Zhao (✉)
State Key Laboratory of Nonlinear Mechanics,
Institute of Mechanics, Chinese Academy of Sciences,
Beijing 100190, China
e-mail: yzhao@imech.ac.cn

Introduction

The well-regarded Young's equation, $\cos\theta = (\gamma_{sl} - \gamma_{sv})/\gamma_{lv}$, defines the balance of the horizontal components of the three interfacial tensions when a liquid droplet is in contact with an ideal flat surface [1]. A specific contact angle (CA) θ can be obtained for a certain liquid–solid–vapor system from the Young's equation. However, one can almost never obtain a unique CA in practice. Instead, the measured CA of a sessile droplet usually lies within a range bounded by the receding and advancing angles θ_r and θ_a, i.e., $\theta_r \leq \theta \leq \theta_a$. The advancing and receding angles are defined as the maximum and the minimum of the CA without increasing the solid–liquid interfacial area, which means that they are measured just before the

motion of the contact line (CL). The difference between the advancing and the receding CAs is defined as the contact angle hysteresis (CAH) [2].

CAH is of significant current scientific interest, not only for its important contribution to understanding of the wetting mechanism, but also due to many technological applications, such as self-cleaning surfaces preparation, oil recovery, filtration and impregnation of textiles, and so on [3]. In the past several decades, CAH has been studied extensively in experiments [4–7] and theoretical analysis [8–10]. According to the conventional definition, CAH is related to the pinning of the CL. Thus, the sources of CAH concern the properties of the solid substrate as well as the liquid. Concerning the substrate, the surface roughness and defects [6], chemical heterogeneities [8], liquid penetration [11], and surface deformation [12] have been discussed. Besides, gradient of chemical potential along the surface is associated with the gradient of surface curvature [13] and thereby it contributes to the CAH. For the liquid properties, it has been found that CAH increases with decreasing chain length of the liquid molecule [5]. CAH is also sensitive to the volume fraction of the microbead suspension [14]. Experiments on CAH were carried out under various situations such as electrowetting-on-dielectric [15] and asymmetric vibration [16]. Recently, Bormashenko et al. presented an ingenious experimental technique to measure CAH based on the slow deformation of the droplet [3]. The appearance of CAH would affect the evaporation mode of the droplet. Large CAH leads to a constant contact area of the droplet until the receding angle is reached [17, 18]. This phenomenon is associated with the "coffee ring effect" [19]. If the CAH is large enough, a pattern would be formed near the pinned CL of the

droplet after its evaporation. Otherwise, it is not easy to observe the coffee ring effect because the CL cannot be pinned. Various theoretical models related to the CAH have been proposed, mainly focusing on the surface roughness and heterogeneity [8]. Even for the substrates without any physical or chemical heterogeneity, an intrinsic CAH can be observed [9]. Extrand derived a thermodynamic expression for free energy of CAH, in which the advancement and recession of CL was modeled as an adsorption and desorption process [10].

Recent advances in microfluidic and nanofluidic technology have promoted the manipulation of much smaller droplets and a wide use of soft materials. For the dynamic behavior of the nanodroplet, the effect of disjoining pressure resulting from van der Waals and electrostatic forces should be included [2]. From a physical perspective, CAH can be regarded as a measure of energy dissipation in response to an exerted force [20] or to a resistive force during the flow of the droplet [21]. If a nanodroplet alters its shape in response to an applied force, the presence of the disjoining pressure promotes the advancement of CL while it hinders the recession of CL. When a droplet is deposited on soft and flexible substrates, the substrate will deform and a ridge along the CL can be pulled up by the vertical component of the surface tension [22–24]. Even for the rigid substrates, Tadmor pointed out that the vertical component of the surface tension would result in molecular reorientation of the surface molecules [25]. Consequently, both the disjoining pressure and the surface deformation of the flexible substrate should be attributed as the sources of the CAH at the nanoscale. Figure 1 summarizes the sources and some influencing factors of the CAH. Molecular level phenomena of CAH and their investigation are becoming

Fig. 1 Sources (*a–e*) and some influencing factors (*f–g*) of the CAH
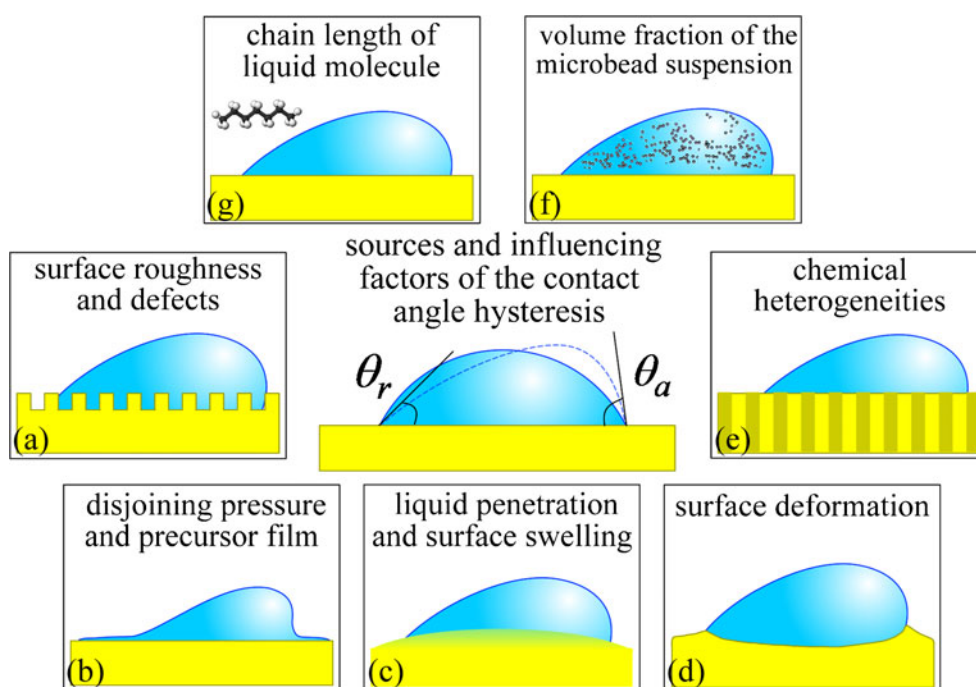
significant. As far as we are aware, there are only a few studies which have reported the investigation of CAH of nanodroplets using molecular dynamics (MD) simulations [26, 27]. Hong and coworkers studied the static and dynamic CAs of water droplets on solid surfaces of different surface energies [26]. Zeng and coworkers carried out MD simulations of CAH for droplets on nanopillared surfaces [27]. However, these MD studies mainly focus on the rigid substrates. In spite of many investigations, the underlying mechanism of CAH and its origin are still not completely understood.

Here, we present MD simulations of liquid droplets in contact with both rigid and flexible substrates with different wetting properties. A body force was applied to the equilibrium droplet to alter its shape until the contact area increased. The motivation for this work is to examine the motion of the CL in the presence of the applied force and further give a description of the correlation between the motion of the CL and the CAH at the nanoscale. The motion of the CL is analogous to the boundary slip behavior. Our previous MD simulations have shown that the boundary slip will not occur unless the shear stress exceeds a critical value, i.e., the critical shear stress (CSS) [28]. Moreover, the CSS depends on the strength of the liquid–solid interactions. In the present study, the motion of the CL is also actuated by the external force to overcome the corresponding energy barrier. Our results indicated that the CA of nanodroplets depends strongly on the wetting properties of the substrate. For the modeled hydrophobic surfaces, the CAH is too small to be detected. Thus, we concluded that there is no obvious CAH due to weak liquid–solid interactions. On hydrophilic surfaces, however, there is strong CAH

due to higher energy barrier. The rest of the paper is organized as follows. In the "Simulation details" section, the simulation models and methodology are described. Then, we present our results related to the CA and CAH of droplets on both rigid and flexible substrates in the "Results and discussion" section. In the "Conclusion" section, we summarize the main conclusions of the present work.

Simulation details

Simulation models

To study the CAH using MD simulations, we first set up the model consisting of a liquid droplet and a solid substrate, as shown in Fig. 2a–c. Here, we used the model presented in the work of De Coninck and Blake [29]. The liquid molecules are 16-atom chains. The advantage of using this kind of liquid molecules is that the viscosity of the liquid can be increased to more realistic values and the evaporation can be considerably reduced. The liquid droplet contains 48,000 atoms, unless otherwise specified. We would discuss the CA dependence on the droplet size and droplets with different diameters would be investigated. Two types of substrates, rigid and flexible, were used. Each substrate was composed of five layers of atoms with a total number of atoms of 80,100, which were modeled based on its face-centered cubic crystal structure and the lattice parameter is 5.56 Å. The mass for all the atoms was assigned to be $m_l=m_s=12 \text{ gmol}^{-1}$. This choice is arbitrary but does not affect the results qualitatively [29].

Fig. 2 **a–c** MD snapshots of liquid droplets placed on rigid substrates with different wetting properties. **d–f** The time-averaged density profiles along the centerline of each droplet are also given. The values of the density are indicated in the legend and the unit is 10^3 kg/m^3. The *dotted lines* are used to fit the shapes of the droplets
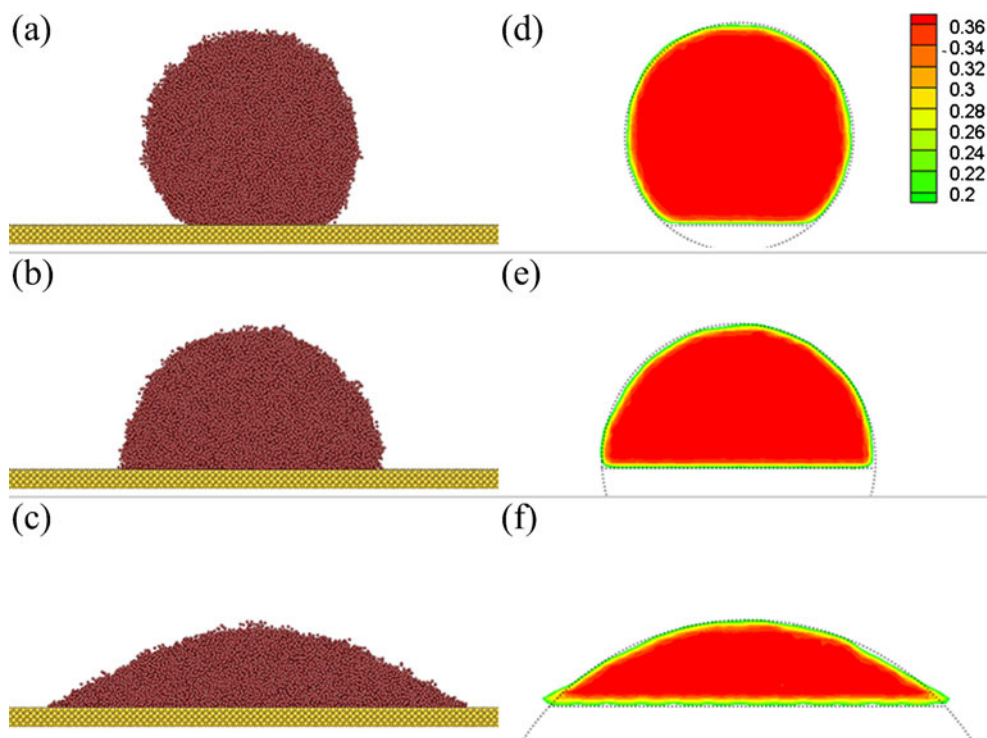
The nonbonded interactions in the droplet–substrate system were described by the Lennard–Jones (LJ) potential:

$$E_{ab}(r) = 4\varepsilon_{ab}\left[\left(\frac{\sigma_{ab}}{r}\right)^{12} - \left(\frac{\sigma_{ab}}{r}\right)^{6}\right] \quad (1)$$

where r is the distance between any pair of atoms. The parameters ε_{ab} and σ_{ab} are related, respectively, to the depth of the potential well and the distance at which the potential is zero. The subscripts a and b denote different atom types, which can be substituted by l (liquid) or s (solid). To simulate the solid substrates with different wetting properties, ε_{ls} was set to be $\varepsilon_{ls}=A\varepsilon_{ll}$, where A was chosen to be 0.3, 0.65, and 1.0. ε_{ll} for liquid–liquid interaction was set to be 4.6×10^{-22} J and $\sigma_{ll}=\sigma_{ss}=3.5$ Å. All the LJ interactions were truncated at a cutoff distance of $2.5\sigma_{ll}$ to accelerate the simulation.

The bond interactions in the liquid droplet between two adjacent atoms within a liquid molecule was modeled by $E(r)=Br^6$, in which the constant was defined as $B = \varepsilon / (\sigma)^6$. For the rigid substrates, each solid atom is fixed to its lattice site. For the flexible substrates, the solid atom is constrained to its lattice site by a harmonic potential, $E_H(r) = C(r - r_0)^2$, in which the spring constant $C = 2.5\varepsilon_{ss}(\sigma)^2/D$. r_0 is the equilibrium position of the atom and D is used to adjust the elasticity of the substrate.

Simulation methodology

We implemented a two-step protocol after the initial configuration of the droplet–substrate system was modeled. In the first step, the equilibrium state of the system was obtained.

The static CA and the deformation of the flexible substrates could be evaluated. After that, we performed MD simulations to determine the CAH. All the simulations were carried out in the NVT ensemble (i.e., the number of atoms N, the volume V, and the temperature T of the system are kept constant). The equations of motion were solved using a velocity Verlet algorithm with a time step of 5.0 fs. The MD simulations presented in this work were performed using the parallelized code LAMMPS [30].

For the equilibrium MD part, the liquid droplet with a cubic shape was initially placed at a certain separation distance (2.0 Å) above the substrate. Then, the system was thermally equilibrated using a Nose–Hoover thermostat for 2×10^6 steps, i.e., 10.0 ns. To minimize the edge effects, periodic boundary condition was imposed in the X and Y directions. We modeled the substrates with large enough dimensions to exclude the interactions between the droplet and its periodic images. During the equilibrium run, the liquid droplet started to wet the substrate and then formed a shape with a certain CA due to the wettability of the substrate. Variations of the CAs of droplets placed on rigid substrates versus time during the equilibrium run were shown in Fig. 3.

Experimentally, there are two conventional methods to measure the CAH. One is the tilting plate method, and the other one is the add/remove volume method. Generally speaking, one cannot adopt the tilting plate approach to investigate the CAH at the nanoscale. This is because, for the nanodroplets, the Bond number is quite small (typically smaller that 10^{-10}), which means that the gravitational effect can be totally neglected compared with the surface tension effect. The second approach to determine the CAH is also not appropriate for MD simulations either since adding or removing molecules during the simulation may cause serious

Fig. 3 Variations of the CAs of droplets versus time during the equilibrium run. The rigid substrates were modeled with $\varepsilon_{ls}=0.3\varepsilon_{ll}$ (open squares), $\varepsilon_{ls}=0.65\varepsilon_{ll}$ (open circles), and $\varepsilon_{ls}=1.0\varepsilon_{ll}$ (open triangles)
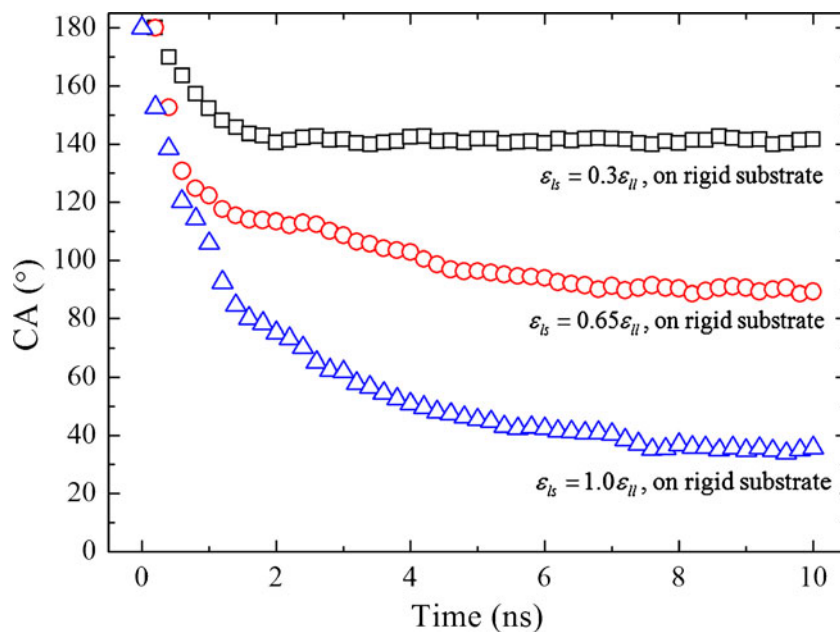
Table 1 Comparison of static CA of droplets on rigid and flexible substrates

	CA (°) on rigid substrate	CA (°) on flexible substrate
$\varepsilon_{ls}=0.3\varepsilon_{ll}$	141.3	158.5
$\varepsilon_{ls}=0.65\varepsilon_{ll}$	90.0	124.5
$\varepsilon_{ls}=1.0\varepsilon_{ll}$	35.4	39.8

computational inefficiency. To determine the CAH in the MD simulations, a body force was thus applied to the droplet after the equilibrium run. A series of body force values were tested to find when the CL started to move. The critical value of the applied force divided by the contact area was defined as the CSS. In the presence of the exerted force, the shape of the liquid droplet would change to exhibit the advancing and receding angles, which is similar to the behavior of the macroscopic droplet in the experiment using the tilting plate method. Based on the MD results, the advancing and receding angles can be determined and, therefore, the CAH can be obtained.

Evaluation of CA, CAH, and the substrate deformation

To evaluate the static CA, as well as the advancing and receding angles of the droplet, the density profiles of the droplet were obtained by time-averaging the MD trajectories of all the liquid molecules. The simulation box was divided into many cubic cells, each with a length scale of 5.0 Å. The density in each cell was averaged every two time steps during the last 2×10^5 steps of each equilibrium run. The liquid domain was specified where the local density was

larger than half of the bulk liquid density. Consequently, the liquid–vapor interface of the droplet can be determined, as shown in Fig. 2d–f. Since we carried out three-dimensional MD simulations, the density profile across the plane through the center of each droplet was extracted. The static CA of the droplet is defined as the angle between the tangential line of the circular droplet surface and the horizontal line representing the surface of the substrate. For the measurement of the advancing and receding angles, two circles with different diameters were used to fit the droplet surfaces at each three-phase contact point. The surface deformation of the flexible substrate was determined in a similar way. After the substrate was divided using a mesh with a grid length of 5.0 Å, the heights of all the substrate atoms were time-averaged.

Results and discussion

The static CA

We first summarize the MD results for the static CA. For the substrates with different wetting properties, the static CAs of the droplets placed on rigid and flexible substrates are listed in Table 1. The static CA depends strongly on the liquid–solid interactions set in the MD simulations. Hydrophobic and hydrophilic surfaces were modeled with $\varepsilon_{ls}=0.3\varepsilon_{ll}$ and $\varepsilon_{ls}=1.0\varepsilon_{ll}$, respectively. The CA on rigid substrate of which the LJ parameter $\varepsilon_{ls}=0.65\varepsilon_{ll}$ is approximately 90.0°. From Table 1, we can find that, for the same liquid–solid interaction, the CA of the droplet on flexible substrate is larger than that on rigid substrate.

To determine the line tension effect in the range of the droplet diameters we studied, we performed simulations of

Fig. 4 Size dependence of the CAs of droplets on flexible and rigid substrates of different wettabilities (*open squares* flexible substrate modeled with $\varepsilon_{ls}=0.3\varepsilon_{ll}$, *solid squares* rigid substrate modeled with $\varepsilon_{ls}=0.3\varepsilon_{ll}$, *open triangles* flexible substrate modeled with $\varepsilon_{ls}=0.65\varepsilon_{ll}$, *solid triangles* rigid substrate modeled with $\varepsilon_{ls}=0.65\varepsilon_{ll}$, *open circles* flexible substrate modeled with $\varepsilon_{ls}=1.0\varepsilon_{ll}$, *solid circles* rigid substrate modeled with $\varepsilon_{ls}=1.0\varepsilon_{ll}$)
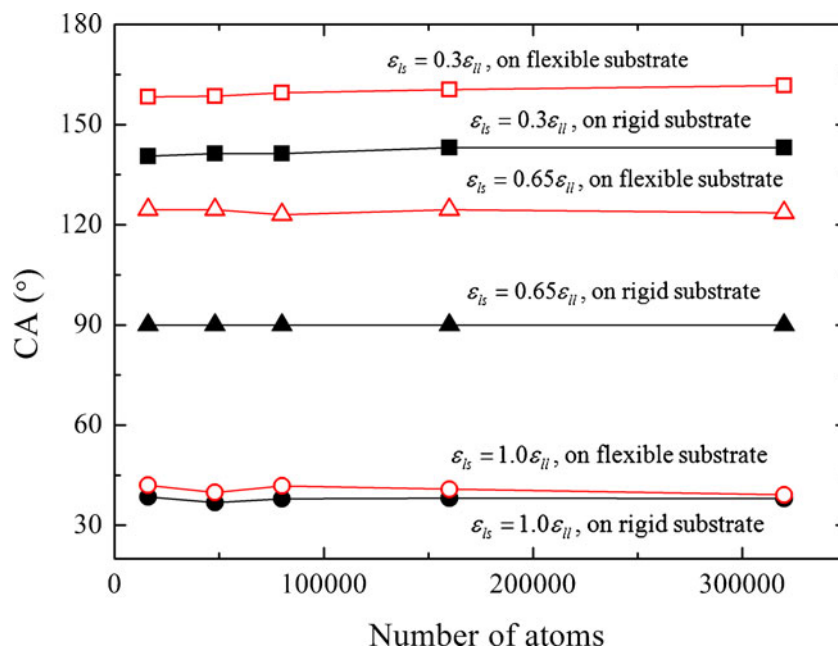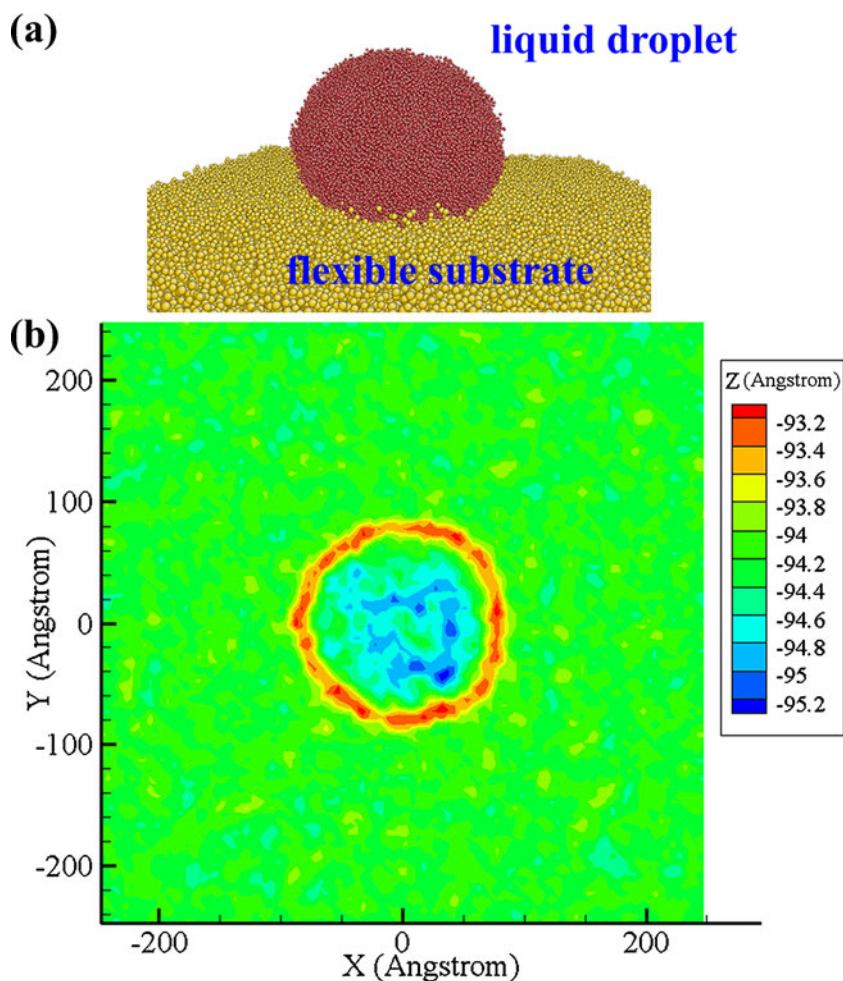
droplets with different sizes (16,000, 48,000, 80,000, 160,000, and 320,000 atoms). The corresponding CAs were shown in Fig. 4. It can be observed that the variation of the CA for different droplet sizes is <3°. These results are consistent with MD results of water droplet containing 12,000–100,000 molecules placed on nanopillared surfaces [27]. Thus, we concluded that the line tension effect was limited for the droplet we studied. These results clearly indicate that the line tension has limited effect in the range of droplet diameters we studied. The influence of the line tension effect on the CAH needs to be further examined.

The deformation of the flexible substrate

When a droplet is placed on a soft and flexible substrate, the substrate would deform and a ridge appears along the CL, which is induced by the vertical component of liquid–vapor interfacial tension [22–24]. Shanahan and de Gennes [22] proposed theoretical estimation of the height of the ridge as $h^* = \gamma_{lv} \sin\theta / G$, where G is the shear modulus of the substrate. The maximum vertical displacement induced by a droplet placed on the poly(dimethylsiloxane) membrane

Table 2 Calculated CSS and CAH

	On rigid substrates		On flexible substrates	
	CSS (kPa)	CAH (°)	CSS (kPa)	CAH (°)
$\varepsilon_{ls}=0.3\varepsilon_{ll}$	1.9	–	2.1	–
$\varepsilon_{ls}=0.65\varepsilon_{ll}$	10.6	13.2	25.1	16.8
$\varepsilon_{ls}=1.0\varepsilon_{ll}$	32.8	20.9	141.5	25.2

can be on the order of hundreds of nanometers [23, 24]. In Fig. 5, the MD snapshot of the droplet placed on the flexible substrate ($\varepsilon_{ls}=0.65\varepsilon_{ll}$) (a) and the averaged height of the flexible substrate (b) are shown. The height of the ridge was estimated to be about 2 Å, much smaller than the theoretical prediction of Shanahan and de Gennes [22]. The reason for this difference is that there is no size effect in the theoretical prediction. The diameter of the droplet in our simulations is about 20 nm; such droplet cannot pull a ridge with a height of hundreds of nanometers. No obvious ridge was observed for the flexible substrate modeled with $\varepsilon_{ls}=0.3\varepsilon_{ll}$ or $\varepsilon_{ls}=1.0\varepsilon_{ll}$. As the

Fig. 5 **a** MD snapshot of the liquid droplet placed on the flexible substrate modeled with $\varepsilon_{ls}=0.65\varepsilon_{ll}$. **b** The averaged height (Z) of the flexible substrate
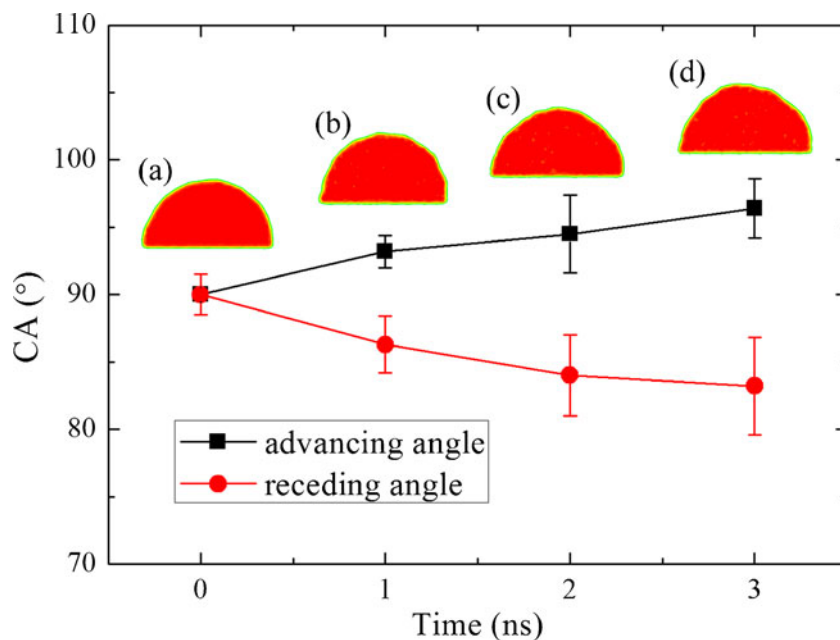
Fig. 6 Variations of the advancing and receding angles versus time for rigid substrate ($\varepsilon_{ls}=0.65\varepsilon_{ll}$) after the body force is applied. The time-averaged density profiles along the centerline of the droplet in response to the exerted force are also given: a t=0 ns; b t=1.0 ns; c t=2.0 ns; d t=3.0 ns

vertical component of the surface tension in these cases is small, so it can not pull up a ridge.

The critical shear stress for the motion of the CL

To determine the CAH, a body force was applied to the liquid droplet in the positive X direction. Then, we monitored the center of the mass as well as the contact area of the droplet. Various parallel MD simulations with different values of the applied body force were performed to determine the CSS which caused the motion of the CL. Here, the CSS for the movement of the droplet is defined as the critical value of the force applied in the MD simulations divided by the contact area of the droplet. The CSS for both rigid and flexible substrates of different wettabilities is listed in Table 2. As the liquid–solid interaction increases from $\varepsilon_{ls}=0.3\varepsilon_{ll}$ to $\varepsilon_{ls}=1.0\varepsilon_{ll}$, the CSS

increases significantly. From Table 2, we find that the response of the CSS to the liquid–solid interaction is not linear. Our previous work reported that the CSS τ_c, which determines the onset of the boundary slip, increases exponentially with the liquid–solid interactions [28]. A similar form for the droplet can be obtained based on the molecular kinetic theory:

$$\tau_c \sim \exp\left(\frac{E_0}{k_B T}\right) \qquad (2)$$

where E_0 is the height of the energy barrier, T is the absolute temperature, and k_B is the Boltzmann constant. The energy barrier results from the interactions between the droplet and the substrate. When considering nanodroplets placed on a flexible substrate, the disjoining pressure effect and the surface deformation would change the potential energy landscape. Thus, τ_c is related to both the disjoining pressure and

Fig. 7 Variations of the advancing and receding angles versus time for rigid substrate ($\varepsilon_{ls}=1.0\varepsilon_{ll}$) after the body force is applied. The time-averaged density profiles along the centerline of the droplet in response to the exerted force are also given: a t=0 ns; b t=1.0 ns; c t=2.0 ns; d t=3.0 ns; e t=4.0 ns
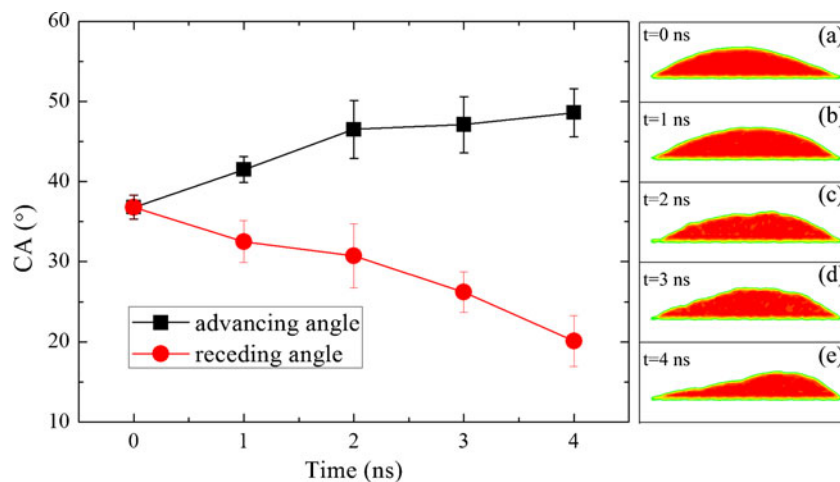
Fig. 8 Variations of the advancing and receding angles versus time for flexible substrate ($\varepsilon_{ls}=0.65\varepsilon_{ll}$) after the body force is applied. The time-averaged density profiles along the centerline of the droplet in response to the exerted force are also given: a $t=0$ ns; b $t=1.0$ ns; c $t=2.0$ ns; d $t=3.0$ ns
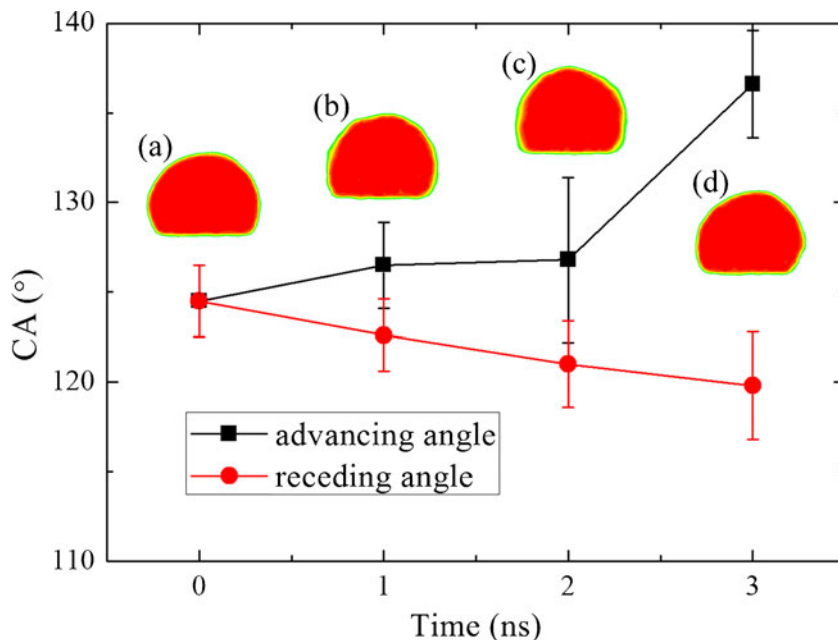
the surface deformation. Here, we propose a simple comparative analysis. The force applied to the liquid droplet for the motion of CL is $\pi\tau_c R^2$, in which R is the droplet base radius. The resistive force resulting from CAH could be estimated by $2R\gamma_{lv}(\cos\theta_r-\cos\theta_a)$ [21]. Balancing the two forces, we find that $\cos\theta_r-\cos\theta_a$ can be written as:

$$(\cos\theta_r - \cos\theta_a) \sim \frac{R}{\gamma_{lv}} \exp\left(\frac{E_0}{k_B T}\right). \quad (3)$$

In some reports, $\cos\theta_r-\cos\theta_a$ is defined as the CAH [4] and the work of adhesion per unit area, w_A, from CAH is expressed to be $w_A=\gamma_{lv}(\cos\theta_r-\cos\theta_a)$ [7]. Anyway, $\cos\theta_r-\cos\theta_a$ represents the trend of the variation of $\theta_a-\theta_r$. Equation 3 gives a molecular level description of the CAH, which involves height of the energy barrier. Actually, E_0 is the activation energy which means the minimum energy required for a liquid

molecule to jump from one equilibrium position to the next. E_0 characterizes the relative height of the potential energy landscape at the CL. The microscopic details, such as the surface roughness, local defects, and surface deformation, contribute to the variation of the height of the energy barrier. It is too complicated to give an analytical expression for E_0 as a function of these parameters. CAH is also found to be proportional to the reciprocal of γ_{lv}, which means that CAH is larger on hydrophilic surfaces without regard to the details of the substrate, such as roughness, defects, or surface deformation.

The CAH of droplet on rigid and flexible substrates

In the presence of the applied body force, the liquid droplet changes its shape. As a result, the advancing CA increases and the receding CA decreases. Figures 6, 7, 8, and 9 show the advancing and receding CAs plotted versus time. Cross-

Fig. 9 Variations of the advancing and receding angles versus time for flexible substrate ($\varepsilon_{ls}=1.0\varepsilon_{ll}$) after the body force is applied. The time-averaged density profiles along the centerline of the droplet in response to the exerted force are also given: a $t=0$ ns; b $t=1.0$ ns; c $t=2.0$ ns; d $t=3.0$ ns; e $t=4.0$ ns
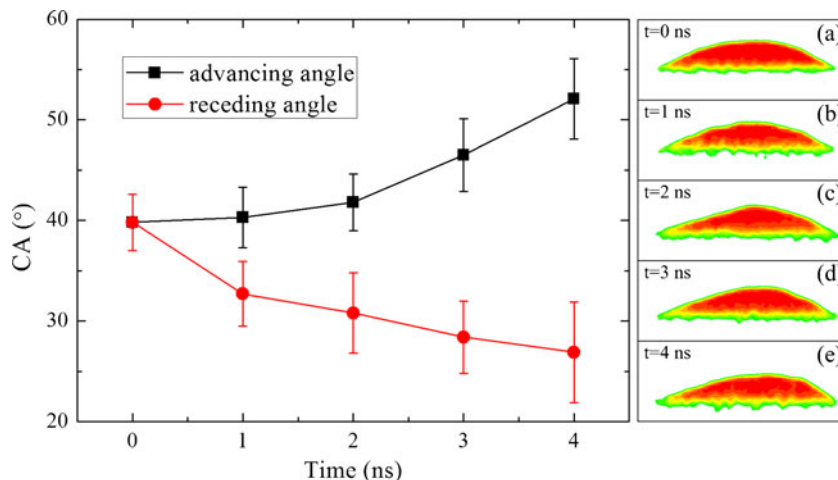
sections of density profiles of the droplet were also given. In Fig. 6, the variations of the advancing and receding angles versus time for the rigid substrate ($\varepsilon_{ls}=0.65\varepsilon_{ll}$) are plotted. The calculated CAH is approximately 13.2°. For the substrate modeled with $\varepsilon_{ls}=1.0\varepsilon_{ll}$, the corresponding CAH is determined to be 20.9°. For the flexible substrate, the CAH values are 16.8° and 25.2° for $\varepsilon_{ls}=0.65\varepsilon_{ll}$ and $\varepsilon_{ls}=1.0\varepsilon_{ll}$, respectively. As discussed in the "Introduction" section, CAH can be regarded as a measure of energy dissipation in response to the exerted force. The way the energy is dissipated at the CL will be critically affected by the body force. For the flexible substrate, the ridge along the CL pulled by the vertical component of the surface tension would increase the energy barrier for the motion of the CL. Consequently, for the same liquid–solid interaction, the CAH of a droplet on a flexible substrate would be larger than that on a rigid substrate, which is in agreement with our MD results. For weak liquid–solid interaction ($\varepsilon_{ls}=0.3\varepsilon_{ll}$), it is difficult to determine the advancing and receding CAs since the CL starts to move once the CSS is achieved. Hence, we conclude that the modeled hydrophobic substrate exhibits no CAH in our simulations. This result is consistent with the theoretical model given in Eq. 3.

Conclusion

In summary, the CAH at the nanoscale was studied using MD simulations. Both rigid and flexible substrates with different wettabilities were modeled. The droplet size dependence of the CA was examined and the surface deformation of the flexible substrate was analyzed. The CSS for the motion of the droplet CL and the CAH were calculated from MD simulations. A simple model of CAH was proposed based on the molecular kinetic theory, which includes the liquid–solid interfacial tension and the molecular level description of the activation energy for the motion of the CL. MD results of CAH are consistent with our theoretical model.

References

1. Young T (1805) Philos Trans R Soc London 95:65
2. de Gennes PG (1985) Rev Mod Phys 57:828
3. Bormashenko E, Bormashenko Y, Whyman G, Pogreb R, Musina A, Jager R, Barkay Z (2008) Langmuir 24:4020
4. Extrand CW, Kumagai Y (1997) J Colloid Interface Sci 191:378
5. Lam CNC, Kim N, Hui D, Kwok DY, Hair ML, Neumann AW (2001) Colloids Surf A 189:265
6. Delmas M, Monthioux M, Ondarcuhu T (2011) Phys Rev Lett 106:136102
7. Wang BB, Zhao YP, Yu TX (2011) J Adhes Sci Technol 25:93
8. Joanny JF, de Gennes PG (1984) J Chem Phys 81:552
9. Schwartz AM (1980) J Colloid Interface Sci 75:404
10. Extrand CW (1998) J Colloid Interface Sci 207:11
11. Sedev RV, Petrov JG, Neumann AW (1996) J Colloid Interface Sci 180:36
12. Extrand CW, Kumagai Y (1996) J Colloid Interface Sci 184:191
13. Herring C (1951) In: Kingston WE (ed) Physics of powder metallurgy. McGraw-Hill, New York, pp 143–179
14. Waghmare PR, Mitra SK (2010) Langmuir 26:17082
15. Nelson WC, Sen P, Kim CJ (2011) Langmuir 27:10319
16. Mettu S, Chaudhury MK (2011) Langmuir 27:10327
17. Bormashenko E, Musina A, Zinigrad M (2011) Colloids Surf A 385:235
18. Yu YS, Wang ZQ, Zhao YP (2012) J Colloid Interface Sci 365:254
19. Deegan RD, Bakajin O, Dupont TF, Huber G, Nagel SR, Witten TA (1997) Nature 389:827
20. Rao DN (2003) In: Mittal KL (ed) Contact angle, wettability and adhesion, 3rd edn. VSP, Utrecht, pp 191–210
21. Feng JT, Wang FC, Zhao YP (2009) Biomicrofluidics 3:022406
22. Shanahan MER, de Gennes PG (1986) Comptes Rendus Acad Sci Serie II 302:517
23. Yu YS (2012) Appl Math Mech-Engl Ed 33:1095
24. Yu YS, Zhao YP (2009) J Colloid Interface Sci 339:489
25. Tadmor R (2011) Soft Matter 7:1577
26. Hong SD, Ha MY, Balachandar S (2009) J Colloid Interface Sci 339:187
27. Koishi T, Yasuoka K, Fujikawa S, Zeng XC (2011) ACS Nano 5:6834
28. Wang FC, Zhao YP (2011) Soft Matter 7:8628
29. De Coninck J, Blake TD (2008) Annu Rev Mater Res 38:1
30. Plimpton S (1995) J Comput Phys 117:1